Surface Science 135 (1983) 409–427
North-Holland Publishing Company

THE INTERACTION OF OXYGEN WITH Ni(111) AND THE REDUCTION OF THE SURFACE OXIDE BY CARBON MONOXIDE AND BY HYDROGEN

F. LABOHM, O.L.J. GIJZEMAN and J.W. GEUS

Van 't Hoff Laboratory, University of Utrecht, Padualaan 8, 3584 CH Utrecht, The Netherlands

Received 25 April 1983; accepted for publication 25 July 1983

The interaction of oxygen with Ni(111) has been studied with ellipsometry and AES. The results are in agreement with those of other workers. The same techniques have been used to study the reduction of the surface oxide by hydrogen and by CO at temperatures of 160–260°C and pressures up to 10^{-3} Torr. For the reduction by hydrogen the results are essentially the same as on Ni(100). The reduction by carbon monoxide proceeds readily on Ni(111), in sharp contrast to Ni(100). We describe the reductions by a modified nucleation and growth type mechanism. The actual reaction takes place on oxide free regions of the crystal, between chemisorbed oxygen and dissociated (adsorbed) hydrogen or adsorbed carbon monoxide. At the boundary between oxide covered and oxide free regions of the crystal, oxidic oxygen is converted to (mobile) chemisorbed oxygen. The activation energy for this process is 33 kcal/mol. The apparent activation energy for the reaction between chemisorbed oxygen and carbon monoxide or hydrogen is 4 and 11 kcal/mol, respectively.

1. Introduction

In this paper we report on the oxidation and subsequent reduction of Ni(111) by CO and by H_2.

Whereas the oxidation of Ni(111) has been studied extensively [1–10] relatively little is known about the subsequent reduction of the surface oxide. Dadayan et al. [6] report on the reduction of 0.25 monolayer of chemisorbed oxygen on Ni(111), while no kinetic measurements seem to exist on the reduction by CO on Ni surfaces.

The study of any surface process involving CO is severely perturbed by the action of more or less energetic electrons, which cause the CO to disproportionate [11–14].

Fortunately in ellipsometry, which employs visible light, we have a technique which allows us to determine kinetic data without disturbing the surface reactions. The ability to continuously monitor the surface has allowed us to obtain a very detailed mechanism for the reduction of Ni/O by CO and by H_2. Changes in the surface composition that occur between the start of

evacuation and the attainment of a CO pressure low enough to permit the use of AES have been a key factor in the development of our reaction model.

2. Experimental

The experiments were carried out on Ni(111) single crystals, mounted in a Varian UHV system equipped with facilities for argon ion bombardment and for simultaneous Auger electron spectroscopy and ellipsometry. The base pressure was less than 10^{-10} Torr. The disc shape crystals were spark-cut from 5N nickel rod within 0.5° of the (111) orientation. The angle of incidence of the 10 mW He–Ne laser beam of the ellipsometer ($\lambda = 6328$ Å) was 68°. Only off-null irradiance measurements were performed. AES was used to determine the surface composition before and after gas exposures. Use was made of a Varian cylindrical mirror analyser with an on-axis electron gun, adjusted to yield an anode current of 400 μA at an electron energy of 2 keV. A modulation frequency of 17 kHz and a modulation amplitude of 10 V were used. The cleaning procedure consisted of Ar^+ sputtering at room temperature until AES indicated the surface to be clean. The energy of the Ar ions was 450 eV, the ion current was about 10 $\mu A/cm^2$, and the angle of incidence was 45°. After this the crystal was annealed at 600°C for 10 min. The gases used: O_2 (purity 99.995%), CO (99.99%), H_2 (99.995%) and Ar (99.999%) were supplied by L'Air Liquide. The pressure in the vacuum chamber was measured by a Varian nude-ionization gauge for pressures up to 10^{-3} Torr, for higher pressures a Varian millitorr gauge was used. Both gauges were not in line of sight with the crystal.

3. Results

3.1. Oxidation of Ni(111) by O_2

The effect of adsorption of oxygen of Ni(111) on the ellipsometric parameter Δ is shown in fig. 1. It can be seen that there is little change in Δ up to an exposure of about 20 L (1 L = 10^{-6} Torr s = 1.33×10^{-4} Pa s), after which a sizable change occurs up to $\delta\Delta = 2.25°$. As on Ni(100) this change reflects the formation of an oxide layer some 2.5 layers thick [7–10]. During a number of oxidation experiments we interrupted the oxygen exposure repeatedly by evacuation, in order to obtain the AES oxygen peak height.

When we attempted to correlate $\delta\Delta$ with the Auger oxygen peak height measurements we found a very large scatter in the Auger peak height ratio $h_O(510\text{ eV})/h_{Ni}(848\text{ eV})$ plotted versus $\delta\Delta$ (cf. fig. 2). At the saturation coverage, however, we always observed the same $\delta\Delta$, corresponding to the

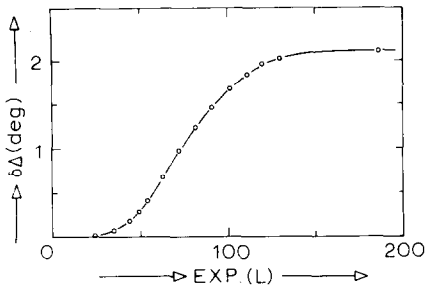

Fig. 1. Oxidation of Ni(111) at room temperature, effect of oxygen exposure on δΔ: (○) experimental; (———) calculated.

same AES peak height ratio. In the pressure range studied (3×10^{-8} to 9×10^{-7} Torr), δΔ depended only on the oxygen exposure.

As on Ni(100) the reaction proceeds in two stages: first a chemisorption stage, followed by a reconstruction and oxidation stage [3–10]. The chemisorption of oxygen leads to a very small change in δΔ, whereas the oxidation is easily measured.

3.2. The reduction of the surface oxide on Ni(111) by CO

The reduction by CO was studied at temperatures between 180 and 260°C and at pressures of 2×10^{-5} to 9.5×10^{-4} Torr. For reductions at high temperatures and low CO pressures the shape of the reaction curves was markedly different from reductions at low temperatures and high CO pressures. While at intermediate T and p the reaction curves were intermediate between these extremes. Some typical reaction curves are given in fig. 3. The

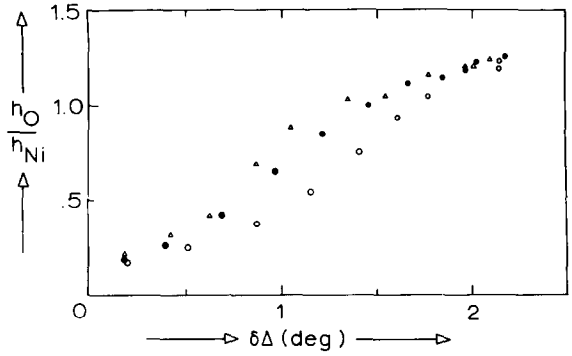

Fig. 2. Plot of the relative Auger signal $h_O(510\ \text{eV})/h_{Ni}(848\ \text{eV})$ as a function of δΔ for three oxidations at room temperature.

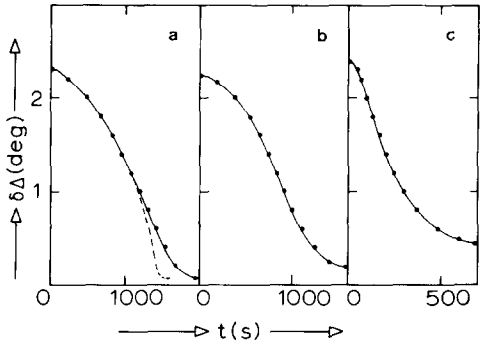

Fig. 3. Reduction of oxidized Ni(111) by CO, effect of the crystal temperature and the CO pressure on the shape of the reaction curves: (a) 240°C, $p_{CO} = 2\times10^{-5}$ Torr; (b) 200°C, $p_{CO} = 5\times10^{-5}$ Torr; (c) 190°C, $p_{CO} = 9.5\times10^{-4}$ Torr; (●) experimental; (— — —) calculated, assuming infinite mobility of chemisorbed oxygen; (———) assuming limited mobility. Only in (a) is there a difference between the two calculations. The reaction curves end at a non-zero value of δΔ because of adsorbed CO.

dependence of the maximum slope of the reaction curves on the temperature is given in fig. 4, for several CO pressures. At each pressure there are two regions, at low temperatures there is an appreciable temperature dependence, while at more elevated temperature the temperature dependence is much weaker. The

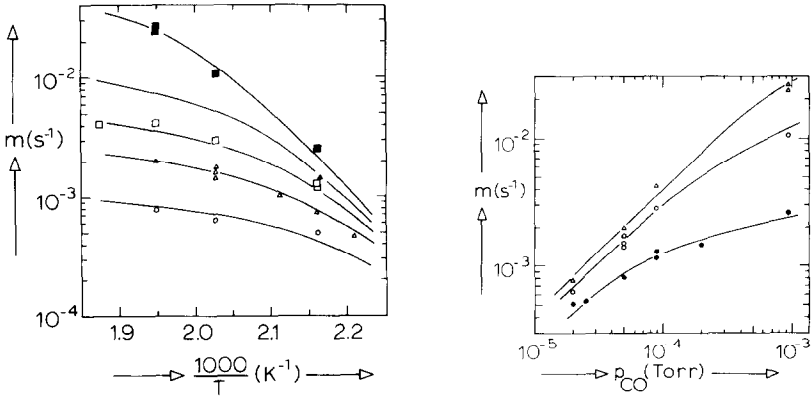

Fig. 4. Temperature dependence of the reduction of oxidized Ni(111) by CO. Arrhenius plot of the maximum slope m of the reaction curves, where $m = (d\delta\Delta/dt)^{max}/\delta\Delta^{max}$: (■) $p_{CO} = 9.5\times10^{-4}$ Torr; (▲) $p_{CO} = 2\times10^{-4}$ Torr; (□) $p_{CO} = 9\times10^{-5}$ Torr; (△) $p_{CO} = 5\times10^{-5}$ Torr; (○) $p_{CO} = 2\times10^{-5}$ Torr. Drawn curves: best fits obtained with the reaction model (see text).

Fig. 5. Pressure dependence of the maximum slope m of the reaction curves for the reduction by CO, where $m = (d\delta\Delta/dt)^{max}/\delta\Delta^{max}$: (●) 190°C; (○) 220°C; (△) 240°C. Drawn curves: best fits obtained with the reaction model (see text).

transition point shifts to higher temperatures with increasing CO pressure. The pressure dependence (fig. 5) shows a similar effect, at low pressures the reaction rate is proportional to the CO pressure, while at high pressures the pressure dependence is much smaller.

After the reaction had been completed (i.e. $\delta\Delta$ had reached a stable value) the system was evacuated, causing the CO present on the surface to desorb, which led to a further decrease in $\delta\Delta$ (cf. fig. 3). The total decrease of Δ was always equal to the increase in Δ accompanying the oxidation, while AES showed the surface to be free of oxygen. We can thus conclude that CO removes the oxygen quantitatively.

If the CO was removed before the end of the reaction, the reaction did not stop instantaneously, but came to a halt rather slowly (see fig. 6). This effect was more pronounced at high CO pressures and at low temperatures, and also if the evacuation took place at a later stage during the reaction. When CO was re-admitted there was no increase in $\delta\Delta$ except when the reaction had been stopped near its completion (cf. fig. 6). In this latter case pumpdown was followed first by a rapid decrease of $\delta\Delta$ and then by a much slower one. On re-admission there was a slow increase of Δ, followed by a slow decrease.

After the reaction the surface was generally free of both oxygen and carbon. In some cases however, some contaminant such as S or C was present. Especially at the lowest temperatures this was accompanied by a marked decrease in the reaction rate.

Due to the fact that the surface could be completely cleaned of oxygen by exposure to CO, it was felt necessary to study the interaction of CO with chemisorbed oxygen only. After exposing the crystal to 10 L of oxygen at room temperature, which caused little change in Δ (less than 0.05°), the UHV chamber was evacuated, the crystal was heated and CO was admitted. On CO admission at pressures below 5×10^{-6} Torr there was a small, stepwise

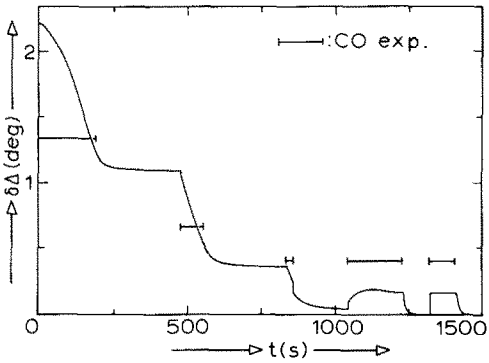

Fig. 6. Effect of evacuation during the reduction by CO at 240°C. CO exposures are at $p_{CO} = 9 \times 10^{-5}$ Torr.

increase of $\delta\Delta$. This increase was smaller at lower CO pressures and at higher crystal temperatures. At higher pressures $\delta\Delta$ increased continuously, even though the CO pressure was constant, until $\delta\Delta$ had reached a stable value. After evacuation AES showed the surface to be clean. Obviously, the continuous increase in Δ is caused by adsorbed CO, which occupies clean nickel sites, after the reaction with chemisorbed oxygen has made these sites available. Some CO adsorption on oxygen filled sites also occurs. From the time it took for $\delta\Delta$ to stabilize, an activation energy of 4 ± 2 kcal/mol was estimated for the reaction between CO and chemisorbed oxygen. At 240°C and $p_{CO} = 5 \times 10^{-5}$ Torr the reaction took about 3 min, while at 47°C this was about 40 min. The reaction rate was first order with respect to the CO pressure. More accurate kinetic measurements were not possible due to the combined effect of CO adsorption on a decreasing amount of chemisorbed oxygen and on an increasing amount of clean nickel.

3.3. The reduction of the surface oxide on Ni(111) by H_2

The reduction by hydrogen was studied at temperatures of 160 to 240°C and H_2 pressures of 5×10^{-7} to 5×10^{-4} Torr, and on two different crystals cut from the same rod, at the same angle. The shape of the reaction curves is shown in fig. 7. In contrast to the reduction by CO there was no saturation of the reaction rate at elevated pressures, even though at the highest pressure the entire reaction took only 15 s. Neither was there any change in the shape of the reaction curves.

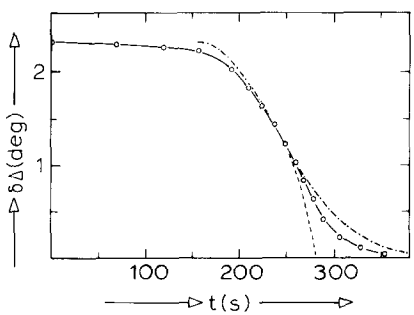

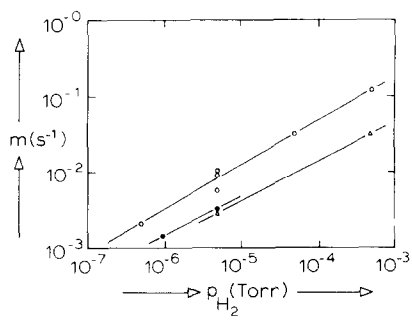

Fig. 7. Typical reaction curve for the reduction of oxidized Ni(111) by H_2 at 220°C and $p_{H_2} = 5 \times 10^{-6}$ Torr: (○) experimental; (·—·—·) calculated with simple island growth model (eq. (2)); (— — —) calculated, assuming infinite mobility of chemisorbed oxygen; (———) calculated, assuming limited mobility.

Fig. 8. Pressure dependence of the maximum slope m of the reaction curves for the reduction by H_2 on two different Ni(111) crystals, where $m = (d\delta\Delta/dt)^{max}/\delta\Delta^{max}$: (●) crystal I at 220°C; (○) crystal II at 220°C; (△) crystal II at 190°C. The slope of the lines is 0.5 ± 0.1.

The measurements on both crystals exhibited the same activation energy (11 ± 1 kcal/mol), even though the absolute rates on the second crystal were about twice as large. Fig. 8 gives the pressure dependence of the reaction rate. On both crystals the reaction rate was proportional to the square root of the hydrogen pressure over the whole pressure range studied.

4. Discussion

4.1. Oxidation

The oxidation of Ni(111) proceeds in the same way as the oxidation of Ni(100) when measured ellipsometrically [14]. The oxidation takes place in two stages. First there is a chemisorption stage, in which about 1/3 of a monolayer of chemisorbed oxygen is deposited on the surface [3,5,8–10]. This is followed by an incorporation stage, during which a NiO layer of about 2.5 monolayers thick is formed via a nucleation and growth process [5,7–10]. During the chemisorption stage there is very little change of $\delta\Delta$, while the growth of the oxide layer gives a change of several degrees (cf. fig. 1).

In contrast to Ni(100) [15] there was no unequivocal relationship between $\delta\Delta$ and the AES oxygen peak height (cf. fig. 2). Whereas $\delta\Delta$ was always the same for the same oxygen exposure, the AES oxygen peak height (normalized with respect to the Ni 848 eV peak) varied erratically. The oxygen peak height at the end of the chemisorption stage, i.e. the point at which $\delta\Delta$ started to increase, reproduced well. The end points of the $\delta\Delta$ versus h_O/h_{Ni} curves also coincide for different oxidation runs at the same crystal temperature. Apparently some kind of reconstruction is still going on on the surface after the gas phase oxygen has been removed prior to the measurement of the AES oxygen peak height. Rieder [7] also concludes that rearrangement still occurs in the oxide layer after evacuation. This may be due to the impact of the AES electron beam, but we have no experimental evidence to support any particular mechanism that causes this rearrangement.

Since for a particular oxygen exposure $\delta\Delta$ reproduced well, while the oxygen AES peak did not, we are convinced that $\delta\Delta$ is a good indicator of the amount of oxygen present on the surface. Moreover, since we could fit $\delta\Delta$ with the same type of equation used earlier [15], we believe that $\delta\Delta$ is linear with the amount of oxide on the surface. We could describe our oxidation curves by

$$\delta\Delta = \delta\Delta^{max}\left[1 - \exp\left(-\alpha p_{O_2}^2 t^2\right)\right], \tag{1}$$

Where $\delta\Delta^{max}$ is the saturation value of $\delta\Delta$, α is a constant depending only on the temperature and p_{O_2} is the gas pressure. For oxidation at room temperature $\delta\Delta^{max}$ was $2.25 \pm 0.15°$ and α was $(2.6 \pm 0.2) \times 10^{+8}$ s^{-2} $Torr^{-2}$, which falls nicely within the range observed by other workers [3,7,10] (3×10^{-9} to 9×10^{-8}).

Fig. 1 shows the comparison between calculated and observed oxidation curves. As on Ni(100), eq. (1) becomes applicable only after the start of the incorporation stage. On Ni(111) the onset of this stage occurred after $(35 \pm 5) \times 10^{-6}$ Torr s. Data from the literature range from 7×10^{-6} [7] to 30×10^{-6} Torr s [10].

For oxidations at higher temperatures the saturation value of $\delta\Delta$ was higher: at 100°C, $\delta\Delta^{max}$ was 2.7°, while at 260°C, $\delta\Delta^{max}$ increased to more than 6°. This measurement was interrupted for fear of permanently damaging the crystal. Since the increase of $\delta\Delta$ during the oxidation was always the same as the decrease accompanying the reduction, regardless of the oxidation and reduction temperatures we can conclude that $\delta\Delta$ depends only on the amount of oxide present on the surface. The increase of the saturation value of $\delta\Delta$ observed for higher oxidation temperatures can therefore be attributed to a thicker oxide layer. This thickening was also observed by Narusawa et al. [8] and Mitchell and Graham [10], but not by, e.g., Holloway and Hudson [3] and by Dadayan et al. [6], probably because AES is not reliable for coverages of several monolayers [8].

4.2. Reduction by CO

4.2.1. Reduction of chemisorbed oxygen

The reduction of half a monolayer of oxygen on Ni(111) is found to be very easy on this crystal plane, in contrast to the same reaction on Ni(100), which did not proceed under our conditions [16]. This reaction exhibited an activation energy of 4 ± 2 kcal/mol and was linear with CO pressure. The Arrhenius plot of fig. 4 exhibits the same activation energy and pressure dependence on the high temperature side. This indicates that this reaction may be involved in the reduction of a surface oxidized to saturation, i.e. covered with nickel oxide.

4.2.2. Reduction of the fully oxidized surface

Looking at the reaction curves of fig. 3 it is tempting to try some modification of island growth kinetics, since this model has been used for the oxidation, and also for the reduction of oxidized Ni(100) by H_2 [15].

Only at high CO pressures and low temperatures, however, can we fit our measurements with the curves predicted by this model. Some modifications are therefore necessary.

Let us summarize the phenomena that our reaction model must explain:
(i) At high temperature and low CO pressures the reaction rate must have a very small activation energy and be first order with respect to the CO pressure.
(ii) At low temperature and high CO pressures the activation energy must be appreciable, but the pressure dependence must be small.
(iii) As one goes from one of these extremes to the other the shape of the reaction curves changes markedly.

(iv) On evacuation during the reaction $\delta\Delta$ does not stabilize instantly, but keeps decreasing for several minutes. On readmission of CO there is no rise in $\delta\Delta$, indicating that no CO is adsorbed.

We shall start with the last item. It is most unlikely that the slow decrease of $\delta\Delta$ after evacuation during the reaction (cf. fig. 6), is caused by the desorption of CO. On the surface that remains after the reaction has been completed, i.e. a clean, but probably somewhat rough Ni surface, the desorption of CO is extremely rapid at our reaction temperatures. Moreover, if only CO desorption takes place (albeit for some mysterious reason very slowly), there is no reason for the CO not to re-adsorb on the surface after re-admission. Since AES shows the surface to contain only oxygen after interrupting a CO exposure, it must be the oxygen on the surface that is somehow responsible for the prevention of the CO adsorption. Let us look at the surface processes in some more detail. During the reaction oxidic oxygen atoms are removed from the edge of islands of "clean" Ni, that thus increase in area. Since only the oxide layer has an ellipsometric effect we can observe only the amount of NiO present on the surface, discounting the effect of CO for the moment. Now suppose that after the evacuation the available clean Ni sites become filled with oxygen, presumably chemisorbed oxygen. Since the only source of oxygen atoms for this process is the oxide layer, the amount of NiO on the surface would decrease, leading to the observed decrease in $\delta\Delta$. This process would stop when all the clean Ni sites available on the island are covered with (chemisorbed) oxygen. As can be seen from fig. 6, evacuation in the beginning of the reaction causes a smaller decrease in $\delta\Delta$ than in case of evacuation in a later stage of the reaction. This supports our hypothesis that oxidic oxygen is converted into chemisorbed oxygen on initially bare nickel islands, whose area is larger in the latter case. Since the chemisorption stage of the oxidation process stops at about 1/3 of a monolayer of oxygen, it would be reasonable to suppose that here this is also the case. This hypothesis is not unreasonable as, according to calculations on Ni clusters, chemisorbed oxygen has a lower energy than oxygen in the oxide layer [17]. Oxygen atoms leaving the oxide layer thus may acquire a considerable kinetic energy; they are "hot" [18]. Liu et al. [9] also conclude that chemisorbed oxygen on Ni(111) is quite mobile.

We tested our hypothesis by the following experiment: After the reaction had proceeded normally at 220°C and 5×10^{-5} Torr CO until about half of the oxide had been removed, the system was evacuated. After $\delta\Delta$ had stabilized, the crystal was allowed to cool to 100°C, a temperature at which previous experiments had shown the reaction rate to be effectively zero. On admission of CO $\delta\Delta$ showed no stepwise increase, indicating that no CO was adsorbed, but increased very slowly to a constant value (see fig. 9). The rate of this increase was comparable to the rate at which CO removes chemisorbed oxygen at this temperature, as determined in a separate experiment.

On evacuation, $\delta\Delta$ decreased very rapidly to the value of before the CO

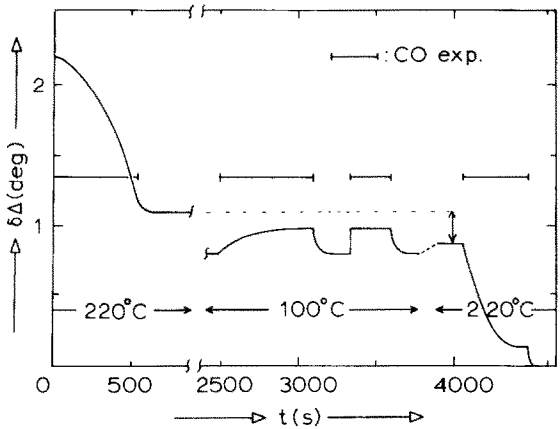

Fig. 9. Experiment to prove oxygen in the oxide layer is converted to (mobile) chemisorbed oxygen on oxide-free regions (islands) of the crystal. At 220°C about half of the oxide is removed by CO. After evacuation the crystal is allowed to cool to 100°C. On re-admission of CO, $\delta\Delta$ increases slowly, indicating that chemisorbed oxygen is removed, thus allowing more CO to adsorb. A second CO exposure at 100°C shows that there is clean Ni available for CO adsorption. On re-heating the crystal to 220°C, $\delta\Delta$ reaches a value below the one before the start of the cooling: some oxide has been converted to chemisorbed oxygen after heating to 220°C (only oxide and CO have an effect on $\delta\Delta$). On admission of CO, $\delta\Delta$ shows no increase, indicating that the clean Ni surface is again covered with chemisorbed oxygen. CO exposures are at $p_{CO} = 5 \times 10^{-5}$ Torr.

exposure, proving that no oxide had been removed at this temperature of 100°C. When we then re-admitted CO, $\delta\Delta$ increased stepwise to the same constant value mentioned before. On re-heating the crystal to 220°C (in vacuum), $\delta\Delta$ reached a value slightly below the start of the experiment, indicating that a small amount of surface oxide had disappeared (see fig. 9).

Since the surface at 100°C did not adsorb any CO until after a considerable CO exposure, we believe this to be clear evidence that initially this surface was covered by an oxide layer, containing Ni islands on which half a monolayer of chemisorbed oxygen was present. Since at 100°C only chemisorbed oxygen reacts with CO, this oxygen was removed, leaving a surface with an oxide layer containing islands of clean Ni, on which the CO could adsorb. At 100°C the clean nickel islands do not become re-covered with chemisorbed oxygen due to the slowness of the breakdown of the oxide layer and the low mobility of oxygen atoms at this temperature.

We are now able to get a detailed picture of what happens during the reaction: At high CO pressures, chemisorbed oxygen is removed very fast, thus leaving the surface of the Ni islands practically free of chemisorbed oxygen. As soon as an oxygen atom at the edge of the oxide layer leaves the oxide for the clean nickel on the island, it reacts with CO and leaves the surface. In this case the breakdown of the oxide layer at the edge of an island becomes rate-limiting and we expect a very small pressure dependence of the reaction rate, exactly as

we observe. Since in this limiting case the reaction rate is strongly temperature dependent, we must conclude that the conversion of oxidic oxygen to chemisorbed oxygen is an activated process. We expect the number of oxygen atoms that leave the edge of the oxide per second to be constant at constant temperature. Therefore the edge of the oxide island moves at a constant speed, and the area of the clean Ni islands increase with time squared. We would thus expect the reaction to follow simple island growth kinetics [15,19]:

$$\delta\Delta = \delta\Delta^{\max} \exp\left[-(k_1 t)^2\right], \tag{2}$$

where $\delta\Delta^{\max}$ is the initial value of $\delta\Delta$, k_1 is a constant depending only on the temperature and t is the time (cf. fig. 3). This equation will be shown to be a limiting case of the general one we shall develop later on.

At the other extreme – high crystal temperature, low CO pressure – the chemisorbed oxygen is supplied very fast, while it is slowly removed. Thus the rate limiting step will be the reaction of chemisorbed oxygen with CO. We observe indeed a reaction rate that is first order with respect to the CO pressure, and that has a (small) activation energy which is the same as the one for the reduction of half a monolayer of chemisorbed oxygen by CO, as determined separately.

If we assume the reaction with chemisorbed oxygen to be first order with respect to the number of chemisorbed oxygen atoms present on the oxide-free islands (N_{ch}) then we get for the change in the number of chemisorbed (N_{ch}) and oxidic (N_{ox}) oxygen atoms:

$$\mathrm{d}N_{ch}/\mathrm{d}t = -\mathrm{d}N_{ox}/\mathrm{d}t - k_2 N_{ch}. \tag{3}$$

Here the first term on the right is the conversion of oxidic oxygen to chemisorbed oxygen, N_{ox} being the number of oxygen atoms present in the oxide layer. The second term describes the first order reaction; the reaction constant k_2 is linear with the CO pressure. We now denote the total area of the crystal by A_{tot}, and the area that is not covered by the oxide layer by A_{isl}, i.e. the total area of the islands, taking their overlap into account. We shall also assume that the chemisorbed oxygen is very mobile, so that we can regard it as being evenly spread out over the part of the crystal where the oxide has been removed, i.e. on the oxide free islands. Thus we can define θ_{ch} as the local chemisorbed oxygen coverage on the islands. Similarly we can define θ_{ox} as the local coverage of oxygen atoms in the oxide layer. In contrast to θ_{ch}, θ_{ox} is constant during the reaction. We can thus write:

$$N_{ch} = \theta_{ch} A_{isl}, \tag{4}$$

$$N_{ox} = \theta_{ox}(A_{tot} - A_{isl}), \tag{5}$$

or, combining these equations with eq. (3):

$$\frac{\mathrm{d}}{\mathrm{d}t}(\theta_{ch} A_{isl}) = \frac{\mathrm{d}}{\mathrm{d}t}\left[\theta_{ox}(A_{tot} - A_{isl})\right] - k_2 \theta_{ch} A_{isl}. \tag{6}$$

Since the conversion of oxidic to chemisorbed oxygen after evacuation eventually stops, there must be some maximum to θ_{ch}, which we shall call θ_{ch}^{max}. This is probably a coverage of 1/3 of a monolayer [3,5,8–10]. In the case we are considering, the chemisorbed oxygen is removed very slowly, so the coverage must be close to θ_{ch}^{max}. Solving eq. (6) with $\theta_{ch} = \theta_{ch}^{max}$ results in:

$$A_{isl}(t) = A_{isl}(t=0)\exp\left(\frac{\gamma}{1-\gamma}k_2 t\right), \tag{7}$$

where $\gamma = \theta_{ch}^{max}/\theta_{ox}$. Evidently $A_{isl}(t=0)$ must be non-zero, otherwise the reaction would not start. Since $\delta\Delta$ is proportional to the area covered by the nickel oxide, $A_{tot} - A_{isl}$, we get:

$$\delta\Delta = \delta\Delta^{max}\left[1 - B\exp\left(\frac{\gamma}{1-\gamma}k_2 t\right)\right], \tag{8}$$

where $B = A_{isl}(t=0)/A_{tot}$ and $\delta\Delta^{max}$ is the value of $\delta\Delta$ for a surface that is completely covered with oxygen (disregarding the (small) effect of adsorbed CO for the moment). Of course this equation must break down when $\delta\Delta$ becomes close to zero. In that case the oxide has almost disappeared and therefore the concentration of chemisorbed oxygen cannot remain close to its maximum value, since its source has run dry. We are now able to understand the behaviour of our Arrhenius plot (fig. 4). At high temperature the removal of chemisorbed oxygen is rate determining. The activation energy is therefore small, and the reaction rate is therefore linear with the CO pressure, just as we found for the reduction of half a monolayer of chemisorbed oxygen. At low temperatures on the other hand, it is the conversion of oxygen in the oxide layer to chemisorbed oxygen that determines the reaction rate. This process is activated, and of course independent of the CO pressure. This explains the steep slope of our Arrhenius plots at low temperatures. They show an appreciable activation energy and a very small pressure dependence. This model is shown schematically in fig. 10a.

We shall now develop our model further to incorporate not only the limiting cases, but also all cases in between.

To develop an equation that describes all our measurements we must establish a connection between θ_{ch} and the rate of growth of our islands. We know that this rate has a maximum for $\theta_{ch} = 0$ and that the rate is zero if θ_{ch} exactly equals θ_{ch}^{max}. It is therefore reasonable to postulate that the growth of nickel plus chemisorbed oxygen islands occurs according to:

$$\mathrm{d}r/\mathrm{d}t = K_1(1 - \theta_{ch}/\theta_{ch}^{max}). \tag{9}$$

The island growth model states that quite generally:

$$A_{isl} = A_{tot}[1 - \exp(-A_{ext})], \tag{10}$$

where A_{ext} is the sum of the areas of all the individual islands, without taking

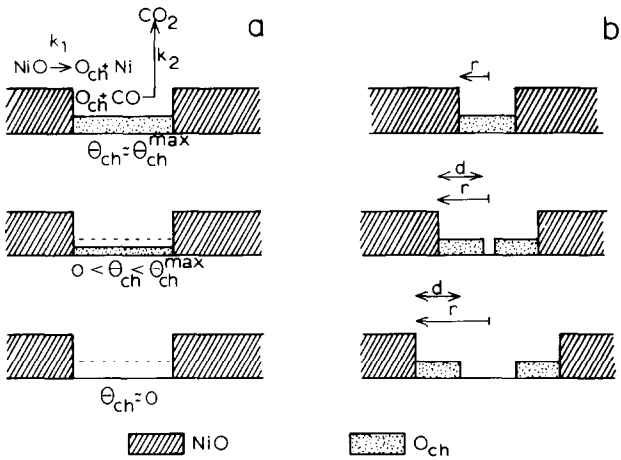

Fig. 10. Schematic drawings of an island growing in the NiO layer during the reduction by CO. At the edge of the oxide oxidic oxygen atoms are converted to (mobile) chemisorbed oxygen (rate constant k_1). The chemisorbed oxygen subsequently reacts with CO (rate constant k_2). The vertical dimension gives an indication of the local concentration of oxygen atoms (not to scale): (— — —) maximum chemisorbed oxygen coverage. (a) Effect of temperature and CO pressure. Upper drawing: at high temperature and low CO pressure the chemisorbed oxygen is supplied fast and removed slowly, the chemisorbed oxygen coverage is therefore near its maximum value, and the reaction with CO is rate-determining. Lower drawing: at low temperatures and high CO pressures the chemisorbed oxygen is removed very fast, and supplied slowly, the chemisorbed oxygen coverage is therefore nearly zero, and the conversion of oxide to chemisobred oxygen is rate-determining. Middle drawing: intermediate case. (b) Effect of allowing an oxygen atom to travel only a distance d away from the edge of the oxide. As long as the radius r of the island is smaller than d (upper drawing) the result is the same as for infinite mobility. For $r > d$ (lower drawings) there is a smaller area available for the chemisorbed oxygen, and therefore the rate of oxygen removal will be lower.

their overlap into account, divided by the total crystal area. For circular islands of radius r, and a density of ρ islands per unit area we would therefore have:

$$A_{ext} = \pi\rho r^2. \tag{11}$$

We will simplify our equations by putting:

$$R^2 = \pi\rho r^2, \tag{12}$$

$$k_1 = \sqrt{\pi\rho}\, K_1. \tag{13}$$

Thus eq. (9) becomes:

$$\dot{R} \equiv \mathrm{d}R/\mathrm{d}t = k_1(1 - \theta_{ch}/\theta_{ch}^{max}), \tag{14}$$

and so

$$\theta_{ch} = \theta_{ch}^{max}(1 - \dot{R}/k_1), \tag{15}$$

while eq. (10) becomes:

$$A_{\mathrm{isl}} = A_{\mathrm{tot}}\left[1 - \exp(-R^2)\right]. \tag{16}$$

Thus

$$N_{\mathrm{ch}} = A_{\mathrm{tot}}\theta_{\mathrm{ch}}\left[1 - \exp(-R^2)\right], \tag{17}$$

$$N_{\mathrm{ox}} = A_{\mathrm{tot}}\theta_{\mathrm{ox}} \exp(-R^2). \tag{18}$$

By doing this we have eliminated the problem that an increase of r^2 has the same effect as an increase of the number of islands. Eqs. (14) to (18) are also made independent of the exact shape of the islands by this substitution. We can now substitute eqs. (15), (17) and (18) into eq. (3) and do some rearranging, which results in:

$$\ddot{R}\left[1 - \exp(-R^2)\right] + \left(k_1 \frac{1-\gamma}{\gamma} + \dot{R}\right) 2R\dot{R} \exp(-R^2)$$
$$-k_2\left(k_1 - \dot{R}\right)\left[1 - \exp(-R^2)\right] = 0, \tag{19}$$

where $\theta = \theta_{\mathrm{ch}}^{\max}/\theta_{\mathrm{ox}}$. It is easily shown that eq. (19) can be solved for $k_1 \to \infty$ and for $k_2 \to \infty$, resulting together with eq. (18) in eq. (8) and eq. (2), respectively. Of course $\delta\Delta$ is proportional to N_{ox}, so if R is known $\delta\Delta$ can be calculated with the aid of eq. (18). Since all our experimental curves had the steepest slope when about half the oxide had been removed, we calculated the slope of the curves given by eq. (19) as a function of k_1 and k_2 for $A_{\mathrm{isl}}/A_{\mathrm{tot}} = 0.5$. For $\gamma = \theta_{\mathrm{ch}}^{\max}/\theta_{\mathrm{ox}}$ we used the value of 0.18 since the oxide layer is about 2.5 layers of NiO thick, which gives $\theta_{\mathrm{ox}} = 1.9$ with respect to the Ni(111) lattice.

Since k_1 is pressure independent and k_2 is linear with CO pressure, holding k_1 constant while varying k_2 simulates a series of experiments done at the same temperature but at different CO pressures. We used the experimental pressure dependence (at three different temperatures) to obtain the values of k_1 and k_2/p_{CO} at those temperatures. These values of k_1 and k_2/p_{CO} exhibited a linear Arrhenius behaviour, indicating that these constants are indeed associated with elementary steps in the reaction. We could describe k_1 and k_2 by

$$k_1 = k_1^0 \exp(-E_1/RT), \tag{20}$$

$$k_2 = k_2^0 p_{\mathrm{CO}} \exp(-E_2/RT), \tag{21}$$

with $k_1^0 = (8.5 \pm 0.5) \times 10^{12}$ s^{-1}, $E_1 = 33 \pm 3$ kcal/mol, $k_2^0 = (1.8 \pm 0.2) \times 10^4$ s^{-1} Torr^{-1} and $E_2 = 4 \pm 0.5$ kcal/mol. A comparison between calculated and observed maximum slopes is given in fig. 4.

We are now able to calculate k_1 and k_2 for any temperature and CO pressure. We used these values to fit our individual reaction curves. For the numerical evaluation of eq. (19) we used the starting condition $\theta_{\mathrm{ch}}(t=0) = \theta_{\mathrm{ch}}^{\max}$, which leads to $\dot{R}(t=0) = 0$ (cf. eq. (14)). $R_0 = R(t=0)$ was varied until the best fit was obtained. In order to obtain good fits it was necessary to use values

for R_0 of 0.25 to 0.45. This would mean that the fraction of the crystal covered by the oxide layer was only 80% to 95%. This is to be expected, when one remembers that the thickness of the oxide layer depends on the oxidation temperatures, the layer being thicker at higher oxidation temperatures [5,8,10]. When one heats a crystal that had been oxidized at room temperature one would expect that the oxide layer wants to get thicker. It can do so only by contracting, thus leaving a larger fraction of the crystal that is oxide free.

How far this process is advanced will depend strongly on the time between the heating of the crystal and the start of the reduction, resulting in erratic fluctuations of $R_0(t=0)$. As expected, the reduction of a crystal that was oxidized at 100°C gave a much smaller value of R_0.

Of course we also have to apply a correction for the adsorption of CO, since CO also has an ellipsometric effect. Eqs. (15) to (19) allow us to calculate both the coverage of chemisorbed oxygen on the islands and the effective area of the islands. Since we know the $\delta\Delta$ caused by adsorbed CO at the end of the reaction, when the surface is oxygen free, we could calculate the amount of adsorbed CO, assuming an inverse linear relation between the coverages of chemisorbed oxygen and the CO coverage:

$$\delta\Delta = \delta\Delta_{ox} + \delta\Delta_{CO}^{end}\frac{A_{isl}}{A_{tot}}\left(1 - \frac{\theta_{ch}}{\theta_{ch}^{max}}\right), \tag{22}$$

where $\delta\Delta$ is the observed value, $\delta\Delta_{ox}$ is the change of $\delta\Delta$ due to the amount of oxide and $\delta\Delta_{CO}^{end}$ is the $\delta\Delta$ due to adsorbed CO at the end of the reaction. More complicated relationships between $\delta\Delta$ caused by CO and θ_{ch} had little influence on the shape of the reaction curves.

The fits we obtained in this way are quite good (cf. fig. 3), except in the limiting case of high temperature and low pressure (see fig. 3a, dashed line). In this case the theoretical curves were too steep when more than half of the oxide had been removed. Apparently our assumption that the oxygen atoms that leave the oxide are able to travel freely across the entire surface of the islands was too drastic. We obtained good fits by assuming that on the average an oxygen atom can travel only a finite distance d away from the edge of the island.

This means that the circular islands are replaced by "rings" of width d, major radius r and minor radius $(r-d)$ (cf. fig. 10b). The area potentially available for chemisorbed oxygen will be the difference of the area of two sets of islands, having the same centres, and radii r and $(r-d)$, respectively. The number of chemisorbed oxygen atoms will then be:

$$\begin{aligned} N_{ch} &= A_{tot}\theta_{ch}\left\{\exp\left[-\pi\rho(r-d)^2\right] - \exp(-\pi\rho r^2)\right\} \\ &= A_{tot}\theta_{ch}\left\{\exp\left[-(R-D)^2\right] - \exp(-R^2)\right\}, \end{aligned} \tag{23}$$

where $D = d\sqrt{\pi\rho}$. This equation replaces eq. (17) for values of $R > D$. The best

fits were obtained for $D = 0.9$. This modification of our model should not, of course, be taken too literally, since it is most unlikely that such a sharp boundary as shown in fig. 10b exists in reality. It is merely a convenient approximation to enter the finite mobility of the chemisorbed oxygen atoms into our model. There is of course experimental support for this modification, which shows that there must be clean nickel present on the surface near the end of the reaction. We stopped the reaction when almost all the oxide had been removed, and waited until $\delta\Delta$ had stabilized. On re-admission of CO there was an instantaneous increase of $\delta\Delta$, showing that there is clean nickel available for CO adsorption. This increase was much faster than the one observed in the reaction of CO with chemisorbed oxygen (cf. fig. 6).

4.3. Reduction by hydrogen

Having arrived at a detailed model for the reduction by CO that explains all observed phenomena, it would have been most satisfying if the reduction by hydrogen had shown exactly the same behaviour as the reduction by CO. Whereas at sufficiently high pressures the reduction by CO no longer depends on the CO pressure, such behaviour was not shown by H_2. Neither was there the accompanying change in activation energy nor a change in the shape of the reaction curves. All reaction curves for the reduction by H_2 had the same shape as the CO reduction curves in the limit of low pressure and high temperature. These curves could not be fitted by the simple island growth kinetics described by eq. (2), as shown in fig. 7. Since for all hydrogen measurements the activation energy was the same, and the reaction rate was proportional to $p_{H_2}^{1/2}$, we must conclude that the reaction with (dissociated) hydrogen is rate-limiting.

For the reduction by CO we developed a model where "holes" or islands grow in the oxide layer. At the edge of these islands oxygen atoms in the oxide are converted to mobile chemisorbed oxygen. The chemisorbed oxygen subsequently reacts with hydrogen and leaves the surface as H_2O. Since experiment proves the reaction with hydrogen to be rate-determining the conversion of oxidic to chemisorbed oxygen atoms must be fast. The rate of oxygen removal is therefore (at least initially) proportional to the area of the crystal that is covered with chemisorbed oxygen, i.e. the area not covered by the oxide layer.

In the previous section we have shown that in that case the reaction can be described by:

$$\delta\Delta = \delta\Delta^{\max}\left[1 - B\exp\left(\frac{\gamma}{1-\gamma}k_3 t\right)\right], \tag{24}$$

where $\delta\Delta$ is linearly proportional to the amount of oxide present on the surface, $\delta\Delta^{\max}$ is the value of $\delta\Delta$ for a completely oxidized surface and B denotes the fraction of the surface not covered by the oxide at $t = 0$, while γ is

quotient of the (local) chemisorbed oxygen coverage and the (local) oxygen coverage in the oxide layer. The reaction constant k_3 for the overall reaction between adsorbed, dissociated hydrogen and chemisorbed oxygen can be described by:

$$k_3 = k_3^0 p_{H_2}^{1/2} \exp(-E_3/RT), \tag{25}$$

where $k_3^0 = (9.7 \pm 1) \times 10^{-5}$ on the first crystal and $k_3^0 = (19 \pm 2) \times 10^{-5}$ s^{-1} $Torr^{-1/2}$ on the second. On both crystals $E_3 = 11 \pm 1$ kcal/mol. Dadayan et al. [6] report an experimental activation energy of 12 kcal/mol for 0.25 monolayer of chemisorbed oxygen on Ni(111), in good agreement with our value. The reduction by H_2 shows no signs of becoming pressure independent at a reaction rate (defined as the maximum slope of the reaction curve) that is much larger than the maximum reaction rate attainable for the reduction by CO at the same temperature (cf. figs. 5 and 8). It therefore seems that the conversion of oxidic oxygen to chemisorbed oxygen is much easier for the reduction by hydrogen. This may well be caused by the presence of O–H groups on the oxide, as observed on oxidized Ni films and (single) crystal surfaces [20–22].

As in the case of CO it was necessary to assume only limited mobility of oxygen across the surface of the island in order to obtain quantitative agreement with the experiments. The best fits to the experimental curves were obtained for $D = 0.9$ (cf. eq. (23) and fig. 7), the same value as for the reduction by CO.

4.4. Comparison with Ni(100)

4.4.1. Reduction by hydrogen

There is almost no difference in the reduction by hydrogen of Ni(100)/O and Ni(111)/O. The absolute rates differ less than a factor two while the experimental activation energy, the pressure dependence and the shape of the reaction curves are the same. The only difference is the amount of oxide remaining on the surface after the reaction. On Ni(111) the surface was always oxygen free after the reaction, while on Ni(100) a small amount of chemisorbed oxygen (usually less than 0.25 monolayer) remained. This is in accordance with the fact that chemisorbed oxygen is more tightly bound on Ni(100) than on Ni(111) [4,6,9,17].

Since the reduction by CO and H_2 on Ni(111) allowed us to obtain a detailed picture of what happens during the reaction we might take a closer look at the reduction by H_2 on Ni(100). The reaction curves on that plane can indeed be fitted much better by the curves obtained by our reaction model than by the simple island growth kinetics used in our previous publication [15]. The conclusions pertaining to the activation energy of the actual reaction remain unaffected however.

4.4.2. Reduction by CO

The behaviour of oxidized Ni(100) and Ni(111) is radically different. On Ni(100) we were completely unable to remove any oxygen with CO. For coverages of 0.25, 0.5 and 3 monolayers of oxygen no reaction was found for CO pressures up to 10^{-3} Torr and temperatures up to 250°C [16]. Since on Ni(111) the actual reaction takes place between chemisorbed oxygen and CO, it is not surprising that there is no reaction at high coverage. If no chemisorbed oxygen is removed, then the amount of oxide must remain constant. Why, then, does chemisorbed oxygen not react with CO? It is possible, of course, that chemisorbed oxygen, being more strongly bound to Ni(100) than to Ni(111), is therefore less mobile. This is corroborated by the fact that on Ni(100) a small amount of oxygen remained after the reduction, while Ni(111) was always oxygen free. Calculations [17,23] and experimental work [4,9] also imply an inherent difference between chemisorbed oxygen on Ni(100) and Ni(111).

5. Conclusions

The reduction of Ni/O by CO is easy on Ni(111) but very hard on Ni(100). The reduction by H_2 shows little difference between these crystal orientations.

The reduction of fully oxidized Ni(111) by CO can be described by the following model: there are two steps in the reaction mechanism, either of which can be rate determining. The first step is the conversion of oxidic oxygen to mobile chemisorbed oxygen. This step has an activation energy of 33 kcal/mol. The second step is the reaction of chemisorbed oxygen with CO, which has an experimental activation energy of 4 kcal/mol and is linearly proportional to the CO pressure.

For the reduction by hydrogen the first step is much faster than for the reaction with CO, and thus the second step, i.e. the reaction of chemisorbed oxygen with dissociated hydrogen, is rate determining. This reaction has an experimental activation energy of 11 kcal/mol, and the rate is proportional to the square root of the hydrogen pressure.

Acknowledgement

We would like to thank M.M.J. van Zandvoort for his part of the experimental work.

References

[1] A.U. MacRae, Surface Sci. 1 (1964) 319.
[2] A.M. Horgan and I. Dalins, Surface Sci. 36 (1973) 526.
[3] P.H. Holloway and J.B. Hudson, Surface Sci. 43 (1974) 141.
[4] J.E. Demuth and T.N. Rhodin, Surface Sci. 45 (1974) 249.
[5] P.R. Norton, R.L. Tapping and J.W. Goodale, Surface Sci. 65 (1977) 13.
[6] K.A. Dadayan, G.K. Boreskov, V.I. Savchenko, N.N. Bulgakov and M.D. Smolikov, Dokl. Akad. Nauk SSSR 239 (1978) 356.
[7] K.H. Rieder, Appl. Surface Sci. 2 (1978) 74.
[8] T. Narusawa, W.M. Gibson and E. Törnqvist, Surface Sci. 114 (1982) 331.
[9] H.T. Liu, A.F. Armitage and D.P. Woodruff, Surface Sci. 114 (1982) 431.
[10] D.F. Mitchell and M.J. Graham, Surface Sci. 114 (1982) 546.
[11] J.C. Tracy, J. Chem. Phys. 56 (1972) 2736.
[12] H.H. Madden and G. Ertl, Surface Sci. 35 (1973) 211.
[13] J. Verhoeven and J. Los, Surface Sci. 82 (1979) 109.
[14] E.G. Keim, F. Labohm, O.L.J. Gijzeman, G.A. Bootsma and J.W. Geus, Surface Sci. 112 (1981) 52.
[15] P.K. de Bokx, F. Labohm, O.L.J. Gijzeman, G.A. Bootsma and J.W. Geus, Appl. Surface Sci. 5 (1980) 321.
[16] F. Labohm, C.W.R. Engelen, O.L.J. Gijzeman, J.W. Geus and G.A. Bootsma, J. Chem. Soc. Faraday Trans. I, 78 (1982) 2435.
[17] G. Allan and J. Lopez, Surface Sci. 95 (1980) 214.
[18] J. Harris and B. Kasemo, Surface Sci. 105 (1981) L281.
[19] M. Avrami, J. Chem. Phys. 7 (1939) 1103; 8 (1940) 212; 9 (1941) 177.
[20] V. Ponec, Z. Knor and S. Cerny, J. Catalysis 4 (1965) 485.
[21] A. Benninghoven, P. Beckmann, K.H. Müller and M. Schemmer, Surface Sci. 89 (1979) 701.
[22] S. Bourgeois and M. Perdereau, Surface Sci. 117 (1982) 165.
[23] V.A. Sobyanin, N.N. Bulgakov and V.V. Gorodetskii, Reaction Kinetics Catalysis Letters 6 (1977) 125.